Moreno-González, M.; Millán-Cabrera, R.; Concepción Heydorn, P.; Blasco Lanzuela, T.; Boronat Zaragoza, M. (2019). Spectroscopic Evidence and Density Functional Theory (DFT) Analysis of Low-Temperature Oxidation of Cu+ to Cu2+NOx in Cu-CHA Catalysts: Implications for the SCR-NOx Reaction Mechanism. ACS Catalysis. 9(4):2725-2738. https://doi.org/10.1021/acscatal.8b04717

Spectroscopic Evidence and DFT Analysis of Low Temperature Oxidation of Cu^{+} to $Cu^{2+}NO_x$ in Cu-CHA Catalysts. Implications for the SCR-NO_x Reaction Mechanism

Marta Moreno-González,[†,‡] Reisel Millán,[†] Patricia Concepción, Teresa Blasco[*] and Mercedes Boronat[*]

Instituto de Tecnología Química, Universitat Politècnica de València - Consejo Superior de Investigaciones Cientificas, Av. de los Naranjos, s/n, 46022 Valencia, Spain

[‡]Present address: Department of Chemistry, The University of British Columbia, 2036 Main Mall, Vancouver, British Columbia V6H1Z1, Canada

[†]These authors contributed equally to this work

Supporting Information

ABSTRACT: Despite the intense investigation on the NH_3-SCR-NOx reaction mechanism catalysed by small pore Cu-CHA zeolites, neither the rate determining step of the process nor the exact nature of the active sites under reaction conditions are clearly established. In this work *in situ* EPR and IR techniques combined with DFT calculations are applied to the study of the oxidation half-cycle of the NH_3-SCR-NOx reaction on Cu-SSZ-13 and Cu-SAPO-34 catalysts. EPR and IR spectroscopies unambiguously show that Cu^{+} is oxidized to Cu^{2+} at room temperature in the presence of the reaction mixture (NO, O_2 and NH_3) or NO and O_2, producing adsorbed NO_2, nitrites and nitrates. Several pathways are proposed from DFT calculations to oxidize Cu^{+} cations placed in the plane of the 6R ring units of SSZ-13 and SAPO-34 to Cu^{2+}, either by NO_2 alone or by a mixture of NO and O_2, with activation energy barriers lower than 70 kJ mol^{-1}. The results reported here demonstrate that a reaction mechanism invoking the formation of nitrate/nitrite intermediates on copper cations attached to the zeolite framework can be operational in the low temperature region (T < 350 ºC). Moreover, different intermediates, nitrites vs nitrates, are preferentially stabilized depending on the catalyst composition, silicoaluminophosphate vs aluminosilicate.

KEYWORDS: zeolite, chabazite, mechanism, NH_3-SCR-NO_x, EPR, IR, DFT

1. INTRODUCTION

Nitrogen oxides (NO_x) released from stationary power plants and vehicle exhaust cause serious pollution problems with detrimental effects on human health and environment. The increasingly stringent regulations have motivated extensive research for the development of new technologies to reduce NO_x emissions from diesel vehicles, as they are the main contaminants in big cities. Nowadays, the most efficient technology is the selective catalytic reduction (SCR-NO_x) using ammonia (NH_3-SCR-NO_x) as reducing agent. [1,2] Zeolites with transition metal ions are the preferred catalyst because they display high conversion in a wide range of temperatures and of O_2 concentrations.[3-5] In particular, Cu-SSZ-13 zeolite and Cu-SAPO-34 silicoaluminophosphate, both possessing the small pore chabazite (CHA-type) structure have received great attention due to their high activity and selectivity while exhibiting excellent hydrothermal stability.[6-9]

The standard SCR reaction between NO and NH_3 in the presence of O_2 (eq. 1) and also, although to a less extent, the fast SCR reaction relevant when NO_2 is present (eq. 2) have been extensively investigated in the last years using Cu-CHA zeolite as catalyst.

$$4\ NH_3 + 4\ NO + O_2 \rightarrow 4\ N_2 + 6\ H_2O \quad (1)$$

$$4\ NH_3 + 2\ NO + 2\ NO_2 \rightarrow 4\ N_2 + 6\ H_2O \quad (2)$$

Great research effort has been focused on the state and distribution of copper cations in the CHA-type zeolite with the aim of defining the active sites for the SCR reaction and the origin of its high hydrothermal stability. The CHA framework is composed of double 6R (six-membered ring) units, i.e. hexagonal prism, that link to form cavities of 7.4 Å diameter accessible through smaller 8R (eight-membered ring) windows of 3.8 Å diameter (Figure 1). In zeolite Cu-SSZ-13, the most stable location of divalent Cu^{2+} cations and the one firstly populated is the plane of 6R ring units containing two framework Al atoms (Al pairs), while isolated Al sites present in samples with high Si/Al ratio and/or high Cu loading can stabilize $[Cu(OH)]^{+}$ species.[10-12] Therefore, the nature and the location of copper cations in Cu-CHA-type zeolites varies with the amount (Si/Al ratio) and the distribution (isolated or paired) of framework Al sites, which in turn depend on the synthesis procedure and post-synthesis treatments. Nevertheless, isolated Cu^{2+} and $[Cu(OH)]^{+}$ attached to the zeolite framework display similar catalytic performance and are both considered as active sites for the SCR reaction,[13,14] being the only difference that the reduction of Cu^{2+} to Cu^{+} generates a new Brønsted acid site.[9,12,15] As a result of this research, it is now well established that under standard SCR reaction conditions both Cu^{2+} and Cu^{+} oxidation states co-exist and interconvert through a redox mechanism.[16]

Besides the state of copper, much effort has been paid to the NH_3-SCR-NO_x reaction mechanism that is divided into an oxidation and a reduction part, according to the changes in the oxidation state of copper. In the reduction part, NO and NH_3 are necessary to efficiently reduce Cu^{2+} to Cu^{+}.[3,15-18] It is assumed that both molecules coordinate Cu^{2+} enabling the N-N coupling through the formation of H_2NNO (nitrosamine)[12,15,17,19] or NH_4NO_2 as reac-

tion intermediates,[2,20] which decompose giving N_2 and H_2O while Cu^{2+} is reduced to Cu^+ (eq. 3).

$$Cu^{2+} + NH_3 + NO \rightarrow Cu^+ + N_2 + H_2O + H^+ \quad (3)$$

The oxidation part of the mechanism is still controversial and invokes the formation of nitrite/nitrate intermediates.[17] It is supposed that Cu^+ cations react with NO_2 to give nitrite (4) in fast SCR, and with $NO+O_2$ (5) to give nitrate in the standard SCR reaction, being Cu^+ oxidized to Cu^{2+}.

$$Cu^+ + NO_2 \rightarrow Cu^{2+}NO_2^- \quad (4)$$
$$Cu^+ + NO + O_2 \rightarrow Cu^{2+}NO_3^- \quad (5)$$

Nitrate intermediates formed under standard conditions can react with NO to develop NO_2 and nitrites according to equilibrium (6):

$$Cu^{2+}NO_3^- + NO \leftrightarrow Cu^{2+}NO_2^- + NO_2 \quad (6)$$

Then, NO_2 gives reaction (4) and nitrite reacts with NH_3 or NH_4^+ to release water and N_2. Accordingly, the only difference between the reaction pathway of fast and standard SCR is that nitrites are formed in one or two steps, respectively. Within this scheme, the step determining the rate of the SCR reaction is the oxidation of NO on Cu^+.

However, micro-kinetic studies and DFT calculations have questioned the occurrence of the classical route that assumes the formation of nitrite/nitrates on isolated copper sites at low temperature (T < 350 ºC).The standard SCR rate measured on Cu-SSZ-13 zeolites increases linearly with the copper loading for the usual ion exchange level as expected for isolated active sites, but follows a quadratic dependence at very low copper loading deviating from single-site catalyst.[21,22] The apparent activation energy (E_a) of the SCR reaction in the low temperature region (100 – 200 ºC) obtained experimentally is within the range 40-80 kJ mol^{-1}. This value is significantly lower than the E_a = 104 kJ mol^{-1} calculated for the formation of a Cu^{2+} bidentate nitrate species from NO and O_2 according to reaction (5).[17]

The discrepancies depicted above for the low temperature standard SCR reaction on Cu-CHA catalysts have been explained by invoking an alternative mechanism.[22-25] At low temperature, ammonia molecules coordinate copper cations attached to framework oxygen releasing them from their positions to form mobile $[Cu(NH_3)_4]^{2+}$/$Cu^{2+}(NH_3)_3OH$ and $[Cu^+(NH_3)_2]^+$/H^+]/$Cu^+(NH_3)_2$ complexes. The energy barrier calculated for the oxidation of a $[Cu^+(NH_3)_2]/H^+$ single site to $[OH\text{-}Cu^{2+}(NH_3)_2]$ is 175 kJ mol^{-1},[24] too high for the low temperature SCR,[21,23] but the O_2 activation is sensitively lowered on transient dimeric copper species. Indeed, the diffusion of a $Cu^+(NH_3)_2$ through a 8R window to an adjacent CHA cage containing another $Cu^+(NH_3)_2$ has a low E_a of ~35 kJ mol^{-1}, and the reaction of two close $Cu^+(NH_3)_2$ cations with O_2 to give $[Cu^{2+}(NH_3)_2]\text{-}O_2\text{-}[Cu^{2+}(NH_3)_2]$ is energetically favored.[22-24] In the presence of NO, it is possible to form $[Cu^{2+}(NH_3)_2]\text{-}O\text{-}[Cu^{2+}(NH_3)_2]$ with an E_a of 76 kJ mol^{-1} and releasing NO_2 that gives the fast SCR reaction.[24] In this model, the copper-ammonia adducts, acting as the active sites for the reaction, are comparable to those found in homogeneous catalysis but with limited diffusion capability because of the electrostatic interactions with the zeolite framework, and then behave as intermediate between homogeneous and heterogeneous.[12,16,22,24,25] Indeed, transport limitations of more distant $Cu^+(NH_3)_2$ to form dimers explains the quadratic dependence of the SCR rate on Cu-CHA samples with low copper density. It must be noted that the formation of dimers has been ruled out for the fast SCR reaction, which is assumed to occur through monomeric $(O_2N)Cu^+(NH_3)_2$. At high temperature (T > 350 ºC), copper loses its solvation sphere and moves back to attach the zeolite framework occupying preferentially six-membered ring (6R) positions, and Cu-CHA behaves as a single site catalyst. The experimental E_a of ~140 kJ mol^{-1} is consistent with the high E_a calculated for the NO oxidation step on Cu^+ sites stabilized by the zeolite framework, supporting the nitrate/nitrite route at high temperature,[21-25] and explaining the change of the SCR reaction regime observed at T ~350 ºC.[13,17,21]

To summarize, the more accepted mechanism for the NH_3-SCR-NO_x reaction involves the formation of copper-ammonia adducts at low temperature and of nitrates/nitrites at T > 350 ºC. However, in a recent investigation of the C_3H_8-SCR-NO_x reaction by our group, EPR spectroscopy revealed the formation of $Cu^{2+}NO_3^-$ in Cu-Y and Cu-TNU zeolites in the absence of NH_3 even at 25 ºC.[26] This result appears to be in contradiction with the recently proposed reaction model,[22-25] and has been the motivation of this work.

Here, we have investigated the mechanism of the oxidation half cycle of the low temperature NH_3-SCR-NO_x reaction over Cu-CHA zeolites, Cu-SAPO-34 and Cu-SSZ-13, prepared by a direct synthesis procedure that produces samples with a homogeneous distribution of Cu within the crystal and with a Cu/(Al or Si) ratio of ~0.5. *In situ* EPR and IR spectroscopies provide experimental evidence on the formation of $Cu^{2+}NO_2^-$ and $Cu^{2+}NO_3^-$ by oxidation of Cu^+ under reaction conditions ($NO/NH_3/O_2$) or under $NO+O_2$ at low temperature. DFT calculations propose a complete reaction pathway for the development of nitrates/nitrites on isolated Cu^+ sites with an activation energy lower than 70 kJ mol^{-1}, in the range of E_a measured at low temperature. On the basis of experimental and theoretical results it is concluded here that the nitrate/nitrite route on isolated copper cations operates for the low temperature NH_3-SCR-NO_x reaction on Cu-CHA catalysts.

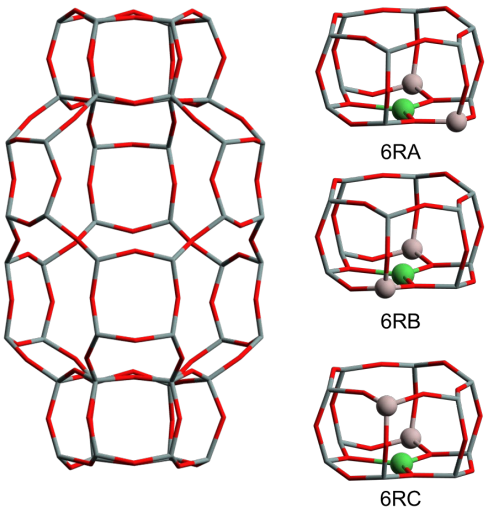

Figure 1. CHA structure showing the 8R windows and D6R units (left) and the three possible distributions of Al pairs in D6R units compensated by a Cu^{2+} cation (right). Si and O atoms are gray and red sticks; Al and Cu atoms are gray and green balls, respectively.

2. RESULTS AND DISCUSSION

2.1. EPR study. Paramagnetic Cu^{2+} ([Ar]$3d^9$) gives EPR hyperfine structures consisting of four components due to the interaction of the unpaired electron with the nuclear spin of copper (I = 3/2). The EPR signals of Cu^{2+} in Cu-zeolites are typically axially symmetric giving hyperfine structure in the parallel region, while the $g_\perp$ component is ill resolved and has low sensitivity to coordination changes, so that they are better characterized by $g_{//}$ and $A_{//}$. With the aim of identifying possible intermediates, *in situ* experi-

ments have been carried out here in order to monitor the changes experienced by Cu^{2+} under the presence of various reactants or under reaction conditions. The Cu-SSZ-13 and Cu-SAPO-34 catalysts were prepared by a one-pot direct synthesis method[27, 28] that allows to obtain samples with a high Cu loading (Cu/(Al or Si) = 0.5, see Table S1) and a homogeneous distribution of Cu within the crystal.

Figure 2 shows the EPR spectra of Cu-SAPO-34 and Cu-SSZ-13 degassed at 450 °C and after the adsorption of reactants (2.6 NH_3/ 2.5 NO/ 1 O_2/ Cu), and Table 1 summarizes the parameters of the EPR signals. Notice that the spectra of Figure 2(a)-(d) are recorded at 230 °C, temperature at which Cu-SAPO-34 and Cu-SSZ-13 are just below maximum conversion in the catalytic test, while the spectra of Figure 2(e) at 250 °C corresponds to maximum conversion (see Figure S1). The spectrum of dehydrated Cu-SSZ-13 (Figure 2(c)) is dominated by a signal attributed to Cu^{2+} coordinated to 3 or 4 framework oxygen atoms of the 6R, labelled site SII (signal Cu^{2+}_{SII}).[29-31] Meanwhile, Cu-SAPO-34 (Figure 2(a)) gives a different signal with parameters $A_{//}$ and $g_{//}$ closer to Cu^{2+} in octahedral coordination and then it is tentatively assigned to highly coordinated Cu^{2+} within the D6R unit (Cu^{2+}_{SI}), or to square pyramid-like $[Cu(H_2O)(O_f)_4]^{2+}$ species on the basis of a recent computational study of EPR parameters.[31] The EPR spectra recorded in the presence of the reaction mixture show a new signal, better resolved in Cu-SSZ-13, labelled here as $Cu^{2+}NO_x^-$ (see Figure 2(b),(d) and Table 1), which was ambiguously assigned to either $Cu^{2+}NO_3^-$ or $Cu^{2+}NO_2^-$ groups in the past and to $Cu^{2+}NO_3^-$ more recently.[17, 29] Nevertheless, according to our modelling of EPR parameters, signal $Cu^{2+}NO_x^-$ is consistent with Cu^{2+} in a distorted square planar geometry resulting from the coordination to two framework oxygens and to two oxygens of either a NO_3^- or a NO_2^- group in a bidentate structure.[31] Besides $Cu^{2+}NO_x^-$, the spectra of the two Cu-CHA samples also contain a signal of Cu^{2+}_{SII} (Figure 2(b),(d)). Cu^{2+}_{SI} signal present in dehydrated Cu-SAPO-34 is not detected suggesting that Cu^{2+} has moved from its original position. The relative intensity of $Cu^{2+}NO_x^-$ decreases when the recording temperature is raised to 250 ºC (maximum NO conversion, see Figure S1), and more at longer heating times (Figure 2(e)). This result suggests that $Cu^{2+}NO_x^-$ are consumed in the SCR reaction with the concomitant reduction of Cu^{2+} to Cu^+. It must be stressed here that no signals from $Cu^{2+}(NH_3)_x$ complexes, previously reported for Cu-SSZ-13 in the presence of only ammonia[32] are observed at any temperature with the reaction mixture. Instead, $Cu^{2+}NO_x^-$ and Cu^{2+}_{SII} are the species present in the catalyst at 230 ºC.

Table 1. EPR parameters of the signals indicated in the spectra of Figures 2-3 measured at 230 °C, corresponding to Cu-SAPO-34 and Cu-SSZ-13 samples submitted to different treatments and their assignment to specific species.

Catalyst	Treatment	$A_{//}$/G	$g_{//}$	$g_{\perp}$	Assignment
Cu-SSZ-13	Dehydrated	134	2.363	2.064	Cu^{2+}_{SII}
	$^{15}NO/^{15}NH_3/O_2$	130	2.362	2.069	Cu^{2+}_{SII}
		147	2.291	-	$Cu^{2+}NO_x^-$
Cu-SAPO-34	Dehydrated	105	2.389	2.066	Cu^{2+}_{SI}
	$^{15}NO/O_2$	142	2.289	-	$Cu^{2+}NO_x^-$
	$^{15}NO/^{15}NH_3/O_2$	130	2.350	2.069	Cu^{2+}_{SII}
		142	2.289	-	$Cu^{2+}NO_x^-$

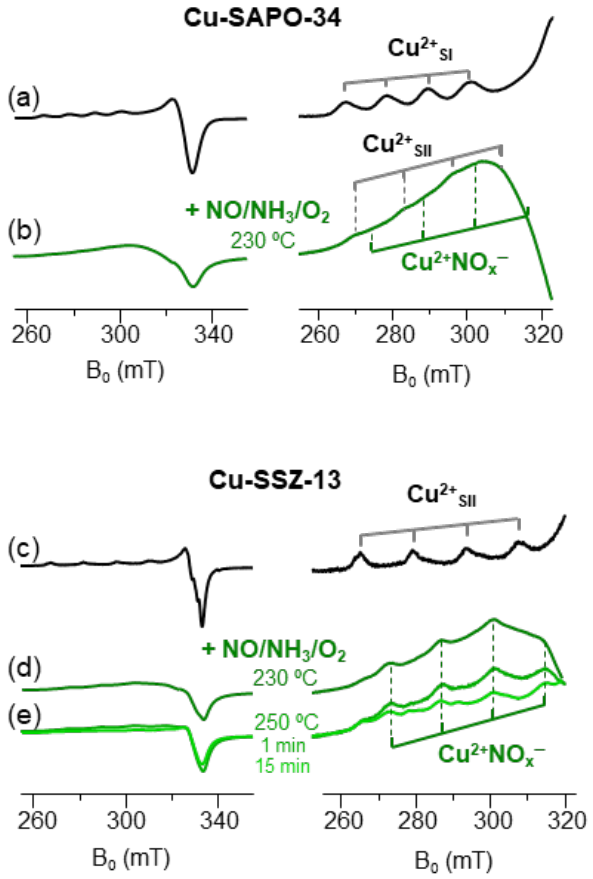

Figure 2. EPR spectra of Cu-SAPO-34 (a), (b) and of Cu-SSZ-13 (c-e) recorded at 230ºC (a-d) or 250 ºC (e) after dehydration at 450 °C (a), (c), and subsequent adsorption of 2.6 NH_3 / 2.5 NO / 1 O_2 / Cu (b), (d), (e). Complete spectrum displayed on the left and magnification of the low-field hyperfine structure on the right side.

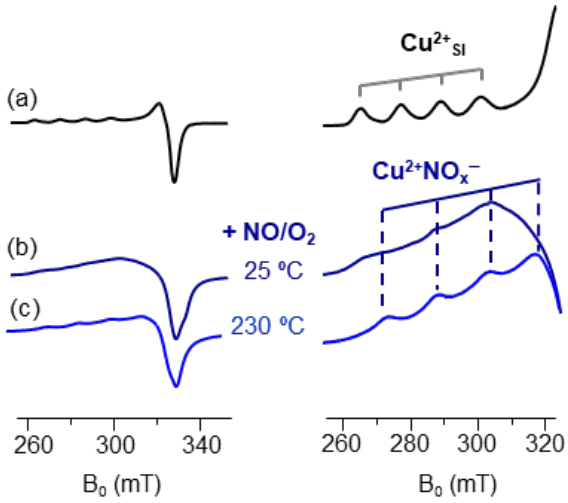

Figure 3. EPR spectra of Cu-SAPO-34 recorded at 230ºC after dehydration at 450°C (a) and recorded at 25ºC (b) and 230ºC (c) after adsorption of 2NO/2O_2/Cu. Complete spectra are displayed on the left and magnification of the low-field hyperfine structure on the right side.

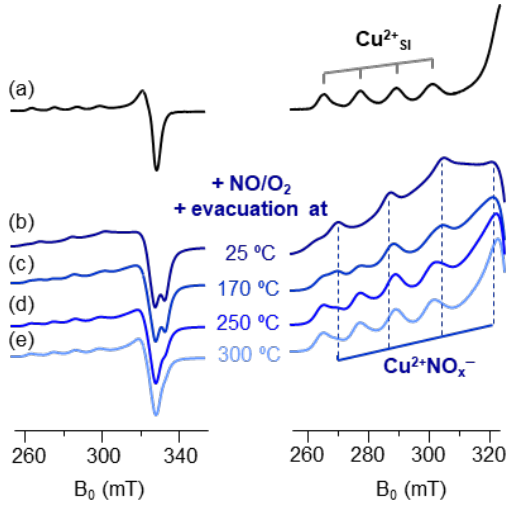

Figure 4. EPR spectra of Cu-SAPO-34 recorded at -170ºC after dehydration at 450°C (a), subsequent adsorption of 2NO/2O_2/Cu and evacuation at 25ºC (b), 170ºC (c), 250ºC (d) and 300ºC (f). Complete spectra are displayed on the left and magnification of the low-field hyperfine structure on the right side.

To get further information on the formation of the $Cu^{2+}NO_x^-$ species, additional experiments were carried out on Cu-SAPO-34, such as the co-adsorption of NO+O_2, or the adsorption of only NO at low temperatures. The spectrum of Cu-SAPO-34 recorded at 25 ºC after co-adsorption of NO+O_2, shown in Figure 3(b) consists of signals of $Cu^{2+}NO_x^-$ and of Cu^{2+}_{SII}. Notice that $Cu^{2+}NO_x^-$ is already formed at 25 ºC, much below the SCR reaction temperature, but is more abundant at 230 ºC. The slight shift of the EPR of $Cu^{2+}NO_x$ signals in Figure 3 is due to the different recording temperature and not to to the presence of distinct species (See Table S2). Comparison of the spectra of Cu-SAPO-34 recorded at 230 ºC with only NO+O_2 (Figure 3(c)) and with NO+O_2+NH_3 (Figure 2(b)), shows that the main difference is that while only $Cu^{2+}NO_x^-$ species are observed in the first case, both $Cu^{2+}NO_x^-$ and Cu^{2+}_{SII} signals are seen when ammonia is also present. This observation suggests that nitrites/nitrates are consumed upon heating in the presence of NO+O_2+NH_3, but not with only NO+O_2, again indicating that these species participate in the SCR reaction.

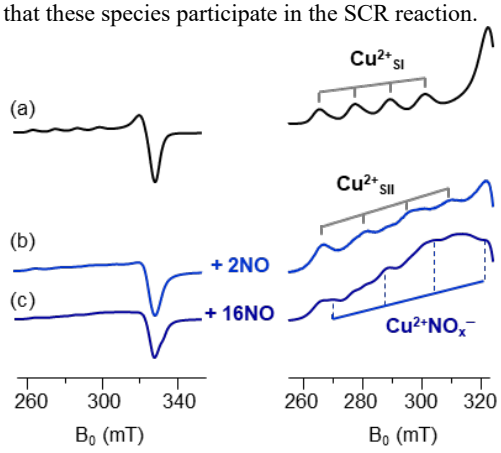

Figure 5. EPR spectra of Cu-SAPO-34 recorded at 25 ºC after dehydration at 450 °C (a) and subsequent adsorption of 2 NO/Cu (b) or 16 NO/Cu followed by evacuation at 25 ºC (c). Complete spectra are displayed on the left and magnification of the low-field hyperfine structure on the right side.

The high thermal stability of the $Cu^{2+}NO_x^-$ in the absence of NH_3 is demonstrated in Figure 4, which shows the EPR spectra recorded at -170 ºC of Cu-SAPO-34 dehydrated at 450 ºC, after the adsorption of NO+O_2, and then subsequent degassing at increasing temperature in the 25–300 ºC range. As the temperature increases, the signal of Cu^{2+}_{SI} progressively grows while that of $Cu^{2+}NO_x^-$ decreases, not disappearing until 300 ºC.

Finally, the adsorption of NO at low temperature (-170 ºC) on Cu-SAPO-34 produces EPR spectra of very low intensity due to the formation of diamagnetic and thus undetectable Cu^{2+}-NO species, and only a weak and practically isotropic peak with g_{iso} = 1.991, assigned to Cu^{+}-NO^{+},[31, 33] (see Figure S2). However, as illustrated in Figure 5(b), when NO is adsorbed at room temperature signals of both Cu^{2+}_{SI} and Cu^{2+}_{SII} are observed, indicating a change in the coordination sphere of some of the Cu^{2+} cations. What it is more interesting, is that increasing the amount of adsorbed NO from 2NO/Cu to 16 NO/Cu provokes the appearance of the $Cu^{2+}NO_x^-$ signal already at 25 ºC, indicating the existence of other processes involving only NO that are able to produce the oxidation of Cu^{+} to $Cu^{2+}NO_x^-$. Indeed, a process involving the formation of $Cu^{+}(NO)_2$ dinitrosyl complexes and their subsequent decomposition into N_2O and a Cu^{2+}-O^{-} species which, in the presence of excess NO, produces $Cu^{2+}NO_2^-$, was proposed to explain the detection of N_2O in Cu-ZSM-5 at room temperature,[34-36] and a similar reaction mechanism was theoretically investigated on Cu-FER with an activation energy barrier for N_2O formation of 109 kJ mol^{-1}.[37, 38]

2.2. DFT study. To explain the EPR observations, the mechanism of the oxidation half-cycle of the NH_3-SCR reaction on Cu-SAPO-34 and Cu-SSZ-13 catalysts was further investigated by means of periodic DFT calculations. Since similar EPR spectra showing $Cu^{2+}NO_x^-$ species are obtained in the absence and presence of ammonia and we are concerned with the possibility that the oxidation pathway might not require ammonia, computations have been made with only NO+O_2. Taking into account the composition, Cu loading and IR characterization of the Cu-SAPO-34 and Cu-SSZ13 samples used in the spectroscopic studies (Figures S3 and S4), the initial active site was assumed to be a Cu^{+} cation placed in a D6R unit containing two Si (or two Al) atoms, with a Brønsted acid site nearby to keep the system neutral. Different distributions of two Si and two Al atoms were considered for Cu-SAPO-34 and Cu-SSZ-13, respectively, the most stable being 6RA site with two Si (or two Al) atoms in the same six-membered ring (Figure 1 and Table S3). The relative energies of all structures investigated are summarized in Table 2, the optimized geometries obtained over site 6RA in Cu-SAPO-34 and Cu-SSZ-13 are depicted in Figures 6-8 and S5-S7, respectively, and the energy profiles are plotted in Figures 9 and S6-S9.

The first pathway considered is the one-step formation of $Cu^{2+}NO_3^-$ by direct reaction of Cu^{+} with NO and O_2 (see structures 1, $TS_{1\rightarrow2}$ and 2 in Figure 6 and energy profile in Figure 9 for Cu-SAPO-34, and Figures S5 and S8 for Cu-SSZ-13). In this process, NO not directly bonded to the active site reacts with O_2 initially activated on the Cu^{+} centre, breaking the O-O bond and forming a bidentate nitrate complex. The calculated activation energy, ~95 kJ mol^{-1}, is similar to those previously reported on Cu-SSZ-13, 104 – 112 kJ mol^{-1}.[17,39] The calculated magnetic moment on the Cu atom, μCu, which is zero in the initial catalyst, increases to 0.231 in Cu-SAPO-34 and 0.197 in Cu-SSZ-13 upon adsorption of molecular O_2 forming structure 1, and to 0.552 and 0.555 in structure 2, confirming the change in the oxidation state from Cu^{+} to Cu^{2+}. Although the reaction is clearly exothermic, this proposed pathway does not take into account the fact that Cu^{+} interacts much stronger with NO forming mono- and di-nitrosyl complexes (structures 3 and 4 in Figure 6) than with O_2, (structure 1 in Figure 6), as demonstrated by IR spectroscopy.[40]

Table 2. Relative stability (in eV) of all structures involved in the oxidation of Cu^+ to Cu^{2+} by $NO+O_2$ with respect to the sum of the energies of Cu-CHA catalyst+$2NO+O_2$. The optimized structures for Cu-SAPO-34-6RA site are depicted in Figures 6-8.

	Cu-SAPO-34		Cu-SSZ-13		
	6RA	6RC	6RA	6RB	6RC
1	-1.170	-1.429	-1.142		
$TS_{1\rightarrow2}$	-0.186	-0.440	-0.175		
2	-3.327	-3.502	-3.297		
3	-1.176	-1.375	-1.175	-1.149	-1.403
4	-2.030	-2.210	-1.982	-1.965	-2.206
5	-2.477	-2.688	-2.443	-2.440	-2.685
$TS_{5\rightarrow6}$	-1.888	-2.117	-1.878	-1.818	-2.117
6	-4.330	-4.546	-4.254	-4.213	-4.520
$TS_{5\rightarrow7}$	-1.753	-1.988	-1.765	-1.746	-2.016
7	-4.238	-4.384	-4.141	-4.109	-4.401
8	-3.786	-4.023	-3.744	-3.676	-3.951
$TS_{8\rightarrow9}$	-3.189	-3.326	-3.095	-3.095	-3.348
9	-4.153	-4.350	-4.123	-4.082	-4.320
10	-3.233		-3.149		
$TS_{10\rightarrow11}$	-3.093		-2.990		
11	-3.558		-3.297		
12[a]	-4.238		-4.141		
$TS_{12\rightarrow13}$[a]	-3.697		-3.540		
13[a]	-4.068		-3.924		

[a]Calculated with respect to the sum of the energies of Cu-CHA catalyst+$2NO+O_2+NO_2$.

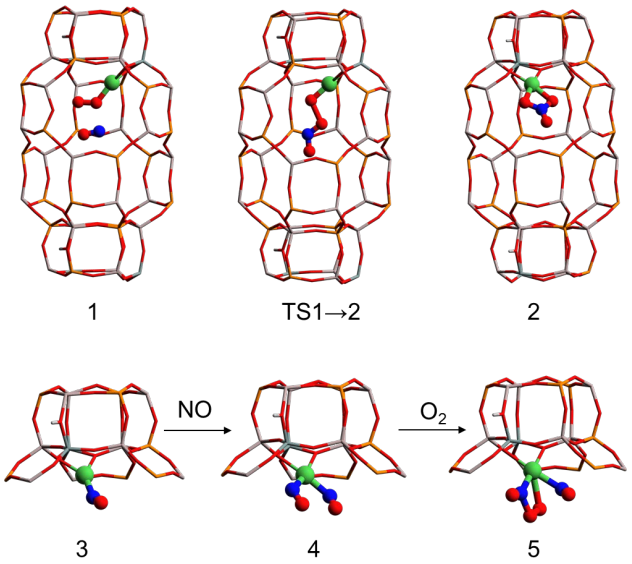

Figure 6. Optimized geometries of NO and O_2 adsorption complexes (1, 3, 4, 5), and of the structures involved in the direct formation of nitrate (2) from $NO+O_2$ in Cu-SAPO-34. Al, P, O, Si, and H atoms in the framework depicted as gray, yellow, red, cyan and white sticks; Cu cations, O and N atoms in the reactant molecules depicted as green, red and blue balls.

Taking this preferential adsorption of NO into consideration, a different pathway was reported by Mao et al.[19] for the oxidation of Cu^+ to Cu^{2+} in Cu-SAPO-34 by reaction of co-adsorbed NO and O_2. This route produces NO_2 and atomic O on copper with activation energies between 83 and 102 kJ mol^{-1}, still quite different from the experimental values. Moreover, the relative stability of structures 1, 3 and 4 (Table 2) and the adsorption constants K_{ads} obtained from the calculated Gibbs free energies at increasing temperatures (Table 3) indicate that O_2 does not compete with NO for the Cu^+ active sites, which will be mono- or bi-coordinated to NO in the whole range of temperature considered. Therefore, reaction paths involving the adsorption of O_2 on Cu^+ sites have not been further considered in the present study. Instead, a second pathway starting from the di-nitrosyl complex 4 was explored, finding a complex in which O_2 adsorbs close to two NO molecules attached to Cu^+ (structure 5 in Figures 6 and S5). In this system, which is described in detail only for site 6RA in Cu-SAPO-34, the O-O bond length has increased to 1.34 Å, one of the O atoms is interacting with one of the N atoms (N-O distance of 1.59 Å), and the other one is close to the Cu^+ site, (Cu^+-O distance of 2.41 Å). From structure 5, two different transition states of comparable stability, $TS_{5\rightarrow6}$ and $TS_{5\rightarrow7}$, lead to formation of two NO_2 molecules interacting with the copper cation in different way (structures 6 and 7 in Figure 7). In $TS_{5\rightarrow6}$ the O-O bond length increases to 1.63 Å, while each of the two O atoms of adsorbed O_2 approaches one N atom of adsorbed NO at optimized O-N distances of 1.39 and 1.41 Å. This way, after O-O bond dissociation, two NO_2 molecules attached to Cu^+ through the N atom are obtained (structure 6 in Figure 7) with an activation energy of 57 kJ mol^{-1}. In $TS_{5\rightarrow7}$ as the O-O bond lengthens to 1.63 Å, one of the O atoms of O_2 gets inserted into the Cu^+-N bond (optimized Cu-O and O-N distances of 1.85 and 1.69 Å, respectively). In this process, a nitrite-like fragment O-bonded to Cu^+ is obtained together with NO_2 interacting through the N atom (structure 7 in Figure 7) with a calculated E_a of 70 kJ mol^{-1}. Rotation of the nitrite fragment in structure 7 produces a less stable system 8 from which nitrate co-adsorbed with NO on Cu^{2+} (structure 9 in Figure 7) is obtained by means of a O transfer through $TS_{8\rightarrow9}$. The calculated activation energy for this step is 58 kJ mol^{-1} in site 6RA of Cu-SAPO-34, but increases to 101 kJ mol^{-1} if we consider as starting point the most stable complex 7. It should be noted at this point that similar structures and energetics are obtained on the 6RC model of Cu-SAPO-34 and on 6RA, 6RB and 6RC models of Cu-SSZ-13 catalysts (see Figures S6, S8-S11).

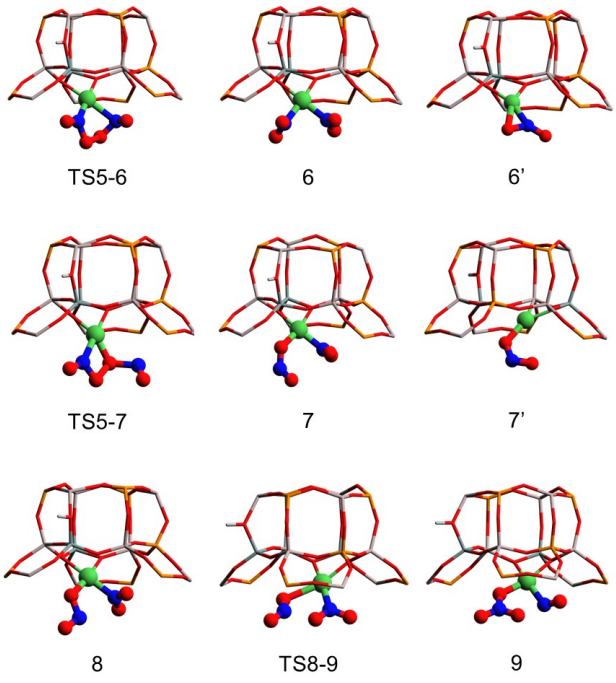

Figure 7. Optimized geometries of the structures involved in the formation of nitrites and nitrates from structure 5 in Cu-SAPO-34. Atom colors described in caption of Figure 6.

Table 3. Calculated adsorption K_{ads} constants of reactant molecules on Cu-SAPO-34 and Cu-SSZ-13 at different T.

	298	373	473	623
Cu-SAPO-34				
$Cu^{+}+NO+O_2 \rightarrow$ **1**	1.43×10^{1}	4.05×10^{-3}	5.92×10^{-6}	2.68×10^{-8}
$Cu^{+}+NO \rightarrow$ **3**	1.14×10^{11}	3.01×10^{7}	3.86×10^{4}	1.39×10^{2}
$Cu^{+}+2NO \rightarrow$ **4**	1.57×10^{15}	5.33×10^{8}	2.71×10^{3}	7.60×10^{-2}
$Cu^{+}+2NO+O_2 \rightarrow$ **5**	9.03×10^{12}	1.48×10^{5}	6.91×10^{-2}	2.85×10^{-7}
$Cu^{+}+NO_2 \rightarrow$ **6'**	1.04×10^{7}	2.21×10^{4}	1.62×10^{2}	3.19×10^{0}
$Cu^{+}+NO_2 \rightarrow$ **7'**	3.34×10^{6}	1.08×10^{4}	1.11×10^{2}	2.43×10^{0}
Cu-SSZ-13				
$Cu^{+}+NO+O_2 \rightarrow$ **1**	8.66×10^{0}	3.01×10^{-3}	5.22×10^{-6}	2.76×10^{-8}
$Cu^{+}+NO \rightarrow$ **3**	2.71×10^{11}	7.13×10^{7}	9.16×10^{4}	3.31×10^{2}
$Cu^{+}+2NO \rightarrow$ **4**	7.29×10^{14}	3.59×10^{8}	2.50×10^{3}	9.30×10^{-2}
$Cu^{+}+2NO+O_2 \rightarrow$ **5**	4.84×10^{11}	8.31×10^{3}	3.85×10^{-3}	1.48×10^{-8}
$Cu^{+}+NO_2 \rightarrow$ **6'**	5.86×10^{6}	1.55×10^{4}	1.33×10^{2}	2.52×10^{0}
$Cu^{+}+NO_2 \rightarrow$ **7'**	2.13×10^{5}	1.34×10^{3}	2.42×10^{1}	8.96×10^{-1}

As regards the change in the oxidation state of Cu, the calculated magnetic moment on the Cu atom in structures 5, 6, 7, 8 and 9 is close to zero, suggesting at first sight that no change in the oxidation state of the active site has occurred. However, this is masked by the fact that both NO and NO_2 have an unpaired electron that modifies the magnetic moment of copper when adsorbed on it. Indeed, the calculated value of μCu in structure 2, with only bidentate nitrate coordinated to Cu, is 0.55. In a similar way, two new structures with only one NO_2 molecule directly attached to Cu, either through the N atom (structure 6') or through the O atom (structure 7') have been optimized. The calculated values of μCu for structures 6' and 7' are, respectively, 0.435 and 0.400 in Cu-SAPO-34, and 0.432 and 0.370 in Cu-SSZ-13 zeolite, indicating that the $Cu^{+} \rightarrow Cu^{2+}$ oxidation has occurred.

Altogether, it is concluded that the Cu^{+}-dinitrosyl complex 4 reacts with O_2, being Cu^{+} oxidized to Cu^{2+} and forming either NO_2 (structures 6, 6' in Figure 7), that is, the catalytic oxidation of NO to NO_2, or $Cu^{2+}NO_2^{-}$ and NO_2 (structures 7, 7' and 8 in Figure 7), with activation energies ranging from 55 to 70 kJ mol^{-1} depending on the nature and distribution of the framework Si and Al sites. These calculated E_a values are comparable to those reported for ammonia solvated $Cu^{+}(NH_3)_2$ complexes as active sites, 60−75 kJ mol^{-1},[23, 24] and in the range of E_a determined experimentally for the low temperature SCR reaction, 40−80 kJ mol^{-1}.

There is also some controversy about the role played by NO_2 in the SCR reaction, especially regarding whether it is generated catalytically on Cu^{+} sites (for example following the 0 → 6 pathway just described) or by direct NO oxidation in the gas phase[41, 42] (reaction 7) or even by NO disproportionation to NO_2 and N_2O within the zeolite voids according to reaction 8:

$$2\ NO + O_2 \rightarrow\ 2NO_2 \qquad (7)$$

$$3\ NO \rightarrow (NO)_3 \rightarrow\ NO_2 + N_2O \qquad (8)$$

An activation energy of 40 kJ/mol has been reported for the rate determining step of the first process,[42] and a similar value of 38 kJ/mol has been now obtained for NO disproportionation (see optimized geometries and relative stability of the species involved in this mechanism in Figure S12).

Next, and since NO_2 can be formed via several pathways, we investigated the possibility of formation of nitrates directly from NO_2 as would be expected to occur under under fast SCR reaction conditions. The initially formed $Cu^{2+}NO_2^{-}$ (structures 7, 7′ in Figure 7) can react with NO_2 (structure 10 in Figure 8) through $TS_{10\rightarrow11}$ and form a bidentate $Cu^{2+}NO_3^{-}$ species and a non-bonded NO molecule (structure 11 in Figure 8) with a really low activation energy barrier, 13 kJ mol^{-1}. In a similar way, a third NO_2 molecule can react with the nitrite fragment co-adsorbed with NO_2 on the Cu^{2+} cation (structure 12 in Figure 8) through transition state $TS_{12\rightarrow13}$ to obtain $Cu^{2+}NO_3^{-}$ together with NO and NO_2 with an E_a value of 52 kJ mol^{-1}. The optimized geometries obtained on Cu-SSZ-13 catalyst, depicted in Figure S7, and the energy profile in Figure S8 are almost identical to those described for Cu-SAPO-34.

It can then be concluded from the DFT study that there are several pathways to form NO_2 and $Cu^{2+}NO_2^{-}$ from $NO+O_2$ and NO alone involving activation energy barriers lower than 70 kJ mol^{-1}, as well as some routes with higher and lower E_a values to obtain $Cu^{2+}NO_3^{-}$.

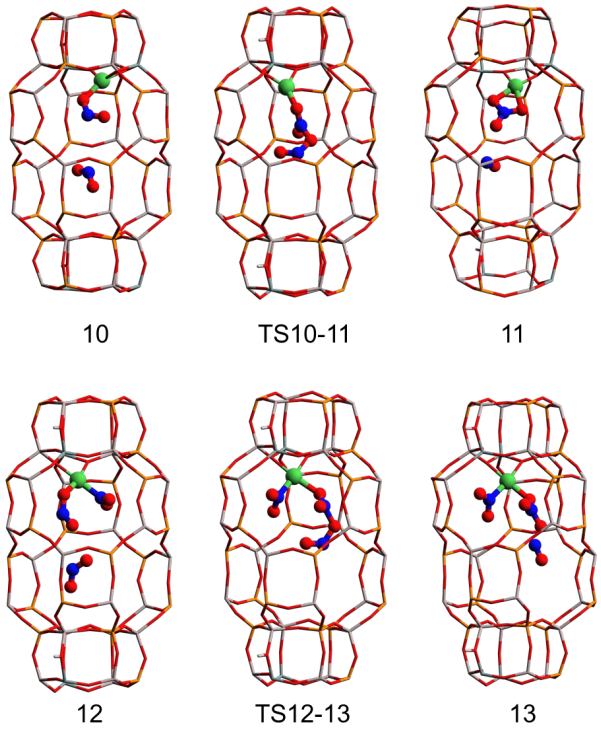

Figure 8. Optimized geometries of the structures involved in the formation of nitrites and nitrates from NO_2 in Cu-SAPO-34. Atom colors described in caption of Figure 6.

To quantify the contribution of each of these pathways to the global formation of NO_2, $Cu^{2+}NO_2^{-}$ and $Cu^{2+}NO_3^{-}$ species under reaction conditions, adsorption K_{ads} and kinetic k_r constants for the most relevant steps were calculated at four temperature values as described in the Computational Details Section. The calculated rate constants k_r for formation of NO_2, NO_2^{-}, and NO_3^{-} species from $NO+O_2$ given in Table 4 increase continuously with increasing temperature. However, the k_r values for the pathways involving the participation of molecules not directly attached to Cu^{+} in the reactant structure and therefore losing some entropy in the transition state, namely 10→11 and 12→13, do not follow a clear and positive trend with temperature. In a similar way, the entropy loss associated to the necessary formation of three-molecular reactant complexes in the non-catalyzed reactions described by equations (7) and (8) results in very low kinetic constants (see Table S4 in the Supporting Information), much lower for the disproportionation than for the NO oxidation reaction. Taking into account the possible enhancement of such reactions within the zeolite voids,[41,42] a small contribution of the non-catalyzed NO oxidation to NO_2 at low T cannot be completely discarded, though it should not be relevant under realistic SCR conditions (see Figure S13 in the Supporting Information).

Table 4. Calculated kinetic constants k_r for key elementary steps on Cu-SAPO-34 and Cu-SSZ-13 at different T (in K).

	298	373	473	623
Cu-SAPO-34				
1→2	9.27×10^{-4}	1.55×10^{0}	7.95×10^{2}	2.19×10^{5}
5→6	2.15×10^{2}	1.49×10^{4}	4.97×10^{5}	1.10×10^{7}
5→7	4.84×10^{1}	9.23×10^{3}	7.40×10^{5}	3.64×10^{7}
8→9	3.98×10^{3}	5.82×10^{5}	4.02×10^{7}	1.91×10^{9}
10→11	2.08×10^{-2}	1.09×10^{-1}	3.11×10^{-1}	8.18×10^{-1}
12→13	5.60×10^{-4}	3.56×10^{-6}	1.28×10^{-4}	3.34×10^{-3}
Cu-SSZ-13				
1→2	1.30×10^{-4}	1.53×10^{-1}	5.59×10^{1}	1.06×10^{4}
5→6	1.59×10^{3}	4.98×10^{4}	8.37×10^{5}	9.68×10^{6}
5→7	9.00×10^{3}	1.86×10^{6}	1.76×10^{8}	1.14×10^{10}
8→9	2.03×10^{1}	2.86×10^{3}	1.73×10^{5}	6.44×10^{6}
10→11	2.59×10^{-3}	1.54×10^{-2}	4.84×10^{-2}	1.39×10^{-1}
12→13	5.89×10^{-10}	8.09×10^{-8}	3.44×10^{-6}	9.75×10^{-5}

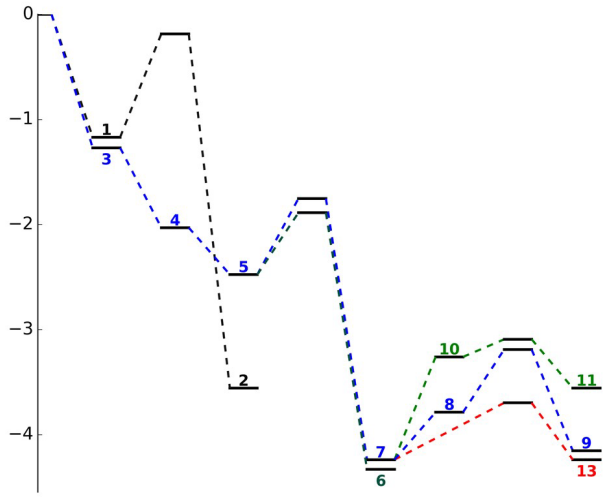

Figure 9. Calculated energy profile for all processes leading to formation of nitrites and nitrates from NO+O_2 and from NO_2 in Cu-SAPO-34 with Cu^+ in site 6R. The optimized structures involved are depicted in Figures 6-8.

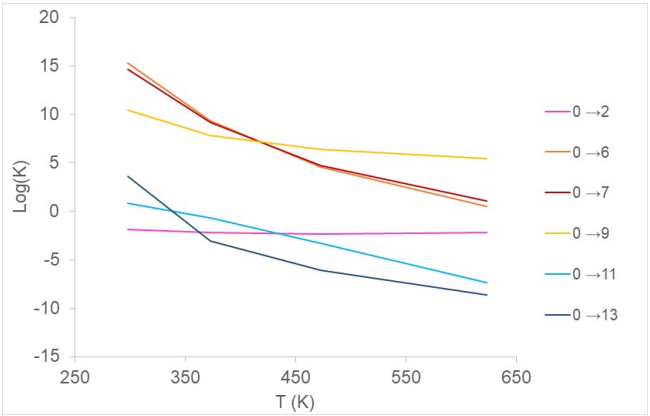

Figure 10. Plot of the logarithm of global rate constants for complete processes leading to formation of $Cu^{2+}NO_2^-$ and $Cu^{2+}NO_3^-$ from Cu^++2NO+O_2 as a function of temperature on Cu-SAPO-34.

Since all the Cu-catalyzed pathways investigated involve consecutive adsorption and reaction steps, which usually follow an opposite trend with temperature, a global rate constant was estimated for each of the complete processes leading to formation of $Cu^{2+}NO_2^-$ and $Cu^{2+}NO_3^-$ from Cu^++2NO+O_2. The plot of the logarithm of such global rate constants as a function of temperature in Figure 10 for Cu-SAPO-34 (and in Figure S14 for Cu-SSZ-13) allows obtaining some clear conclusions. The only pathway previously proposed based on DFT calculations (0→2 process, pink line in Figure 10) has a low contribution to formation of $Cu^{2+}NO_3^-$ in the whole range of temperature considered. In contrast, reaction of 2NO+O_2 yielding either $2NO_2$ molecules (0→6 process, orange line) or nitrite and NO_2 (0→7 process, red line) are always relevant, especially at low temperature. $Cu^{2+}NO_3^-$ is formed mainly through the indirect pathway 0→7→9 (yellow line in Figure 10), and not so much from $2NO_2$ or $3NO_2$ molecules following reactions 0→11 (cyan line) or 0→13 (blue line). Finally, it should be mentioned that NH_3 present under realistic SCR reaction conditions might influence the rates of the oxidation half-cycle by competitively adsorbing at the Cu^+ active sites where NO needs to adsorb, but it is not expected to directly participate in the redox process. Indeed, the adsorption energies of NO and NH_3 on Cu^+ and Brønsted acid sites (see Table S5 in the Supporting Information) indicate that NH_3 interacts preferentially with acid sites forming adsorbed NH_4^+ cations. Taking this into account, we recalculated the oxidation of Cu^+ to Cu^{2+} by 2NO+O_2 following the 5→6 pathway described above, but in the presence of NH_4^+ adsorbed close to the active center (see Figure S15). The new activation and reaction energies are are 75 and -176 kJ mol^{-1}, respectively, not too different from the 57 and -178 kJ mol^{-1} calculated in the absence of NH_3, thus validating the results obtained with only NO and O_2. In subsequent steps of the mechanism, however, the direct participation of NH_3 and/or NH_4^+ is necessary to desorb the nitrite and/or nitrate species from Cu^{2+} forming NO_2NH_4 and/or NO_3NH_4, and to efficiently reduce Cu^{2+} to Cu^+ by reaction of NO+NH_3.

2.3. IR spectroscopy. IR spectroscopy complements EPR and provides relevant information about the chemical nature of the adsorbed species, their interaction strength and geometry. To confirm the theoretical proposals, the interaction of Cu-SAPO-34 with NO_2 (Figure 11), with NO (Figure 12) and with a mixture of NO+O_2 (Figure 13) at 25 ºC and increasing temperatures was investigated using IR spectroscopy. It is generally accepted that IR bands in the 1650 – 1500 cm^{-1} range correspond to nitrite or nitrate species adsorbed on the copper active sites.[20,43-46] However, an accurate identification of these bands is not straightforward and is quite confuse in the bibliography. To assist in the assignation of the IR bands we took into consideration the DFT calculated vibrational frequencies for intermediate structures 6-13, which are summarized in Table S6 in the Supporting Information.

The IR spectra of Cu-SAPO-34 in the presence of only NO_2 at room temperature shows three main bands at 1516, 1578 and 1608 cm^{-1} (Figure 11). Based on bibliography data and the DFT frequencies listed in Table S6, the band at 1608 cm^{-1} is assigned to NO_2 adsorbed on copper. The peak at 1578 cm^{-1} could correspond to bidentate nitrate,[44-46] although it also overlaps with a vibration of nitrite species, and therefore additional experiments were performed to assign this feature. Raman spectra of Cu-SAPO-34 after oxygen activation shows the presence of O_2 species interacting with copper (bands at 475, 417 cm^{-1} for ν(Cu-O) and 1095, 1128 cm^{-1} for ν(O-O))[47] that disappear in an inert flow (Figure S16). These oxygen species may react with NO following the 1→2 pathway discussed previously, forming a bidentate nitrate complex $Cu^{2+}NO_3^-$ (structures 2 and 11). On the other hand, a band at 1578 cm^{-1} is clearly observed in the IR spectra of NO+O_2 adsorbed on a Cu-SAPO-34 sample preactivated in an O_2 atmos-

phere, but is absent when the sample is preactivated in vacuum, where only two bands at 1510 and 1610 cm^{-1} are seen (Figure S17). These results indicate that the band at 1578 cm^{-1} can be safely assigned to $Cu^{2+}NO_3^-$. The signal at 1516 cm^{-1} has not been discussed previously, and according to the DFT simulations it could correspond to a mono-dentate $Cu^{2+}NO_2^-$ (structures 7' and 10 in Figures 7 and 8). Nitrite species show in addition other low frequency IR bands in the 1300 – 1050 cm^{-1} range which are hidden due to the strong absorption of the zeolite lattice vibrations in this region. These IR data confirm the theoretical proposal that Cu^+ is readily oxidized to $Cu^{2+}NO_2^-$ and maybe $Cu^{2+}NO_3^-$ by proper NO_2 adsorption at room temperature.

When Cu-SAPO-34 is exposed to NO alone (Figure 12), IR bands corresponding to N_2O (2224 cm^{-1}), NO^+ (2121 cm^{-1}) and Cu^{2+}-NO (1906, 1885 cm^{-1}) are clearly observed at room temperature together with the three additional IR bands associated to $Cu^{2+}NO_2^-$ (1502 cm^{-1}), $Cu^{2+}NO_3^-$ (1578 cm^{-1}) and adsorbed NO_2 (1608 cm^{-1}). This is in agreement with the EPR results shown in Figure 5 indicating that NO_2 and N_2O are readily formed from NO at all temperatures. At 150ºC Cu-nitrites species (IR band at 1502 cm^{-1}) decompose with the formation of gas phase NO_2 which remains physisorbed as evidenced by the IR peak at 1668 cm^{-1}.

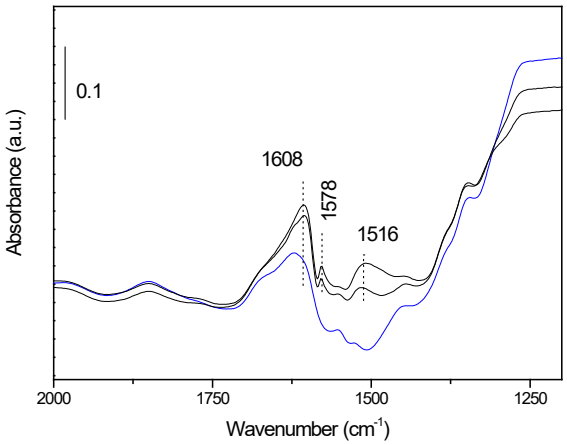

Figure 11. FTIR spectra of Cu-SAPO-34 sample (blue line) and after NO_2 adsorption at increasing coverages (0.1 and 3 mbar). Prior to adsorption the sample was preactivated in O_2 at 350ºC for 2h followed by vacuum at 150ºC for 1h.

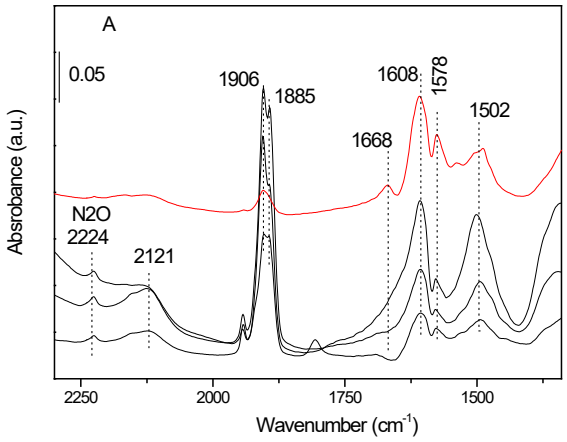

Figure 12. FTIR spectra of NO adsorbed at 25ºC on Cu-SAPO-34 (black line) with time (1, 16, 45min) and after increasing temperature to 150ºC (red line). Prior to adsorption the sample was preactivated in O_2 at 350ºC for 2h followed by vacuum at 150ºC for 1h.

After exposing the Cu-SAPO-34 sample to a mixture of $NO+O_2$ with a $2NO/5O_2/Cu$ molar ratio (see Figure 13A), intense bands associated to nitrite, nitrate and adsorbed NO_2 (1507, 1578 and 1604 cm^{-1}) are observed at room temperature, in addition to N_2O_4 (1742 cm^{-1}), Cu^{2+}-NO (1906, 1887 cm^{-1}), NO^+ (2121 cm^{-1}), N_2O (2223 cm^{-1}) and NO_2 (1668 cm^{-1}) as previously described. Notice the presence of two new features at 1623 and 1298 cm^{-1} that, according to our DFT results, would correspond to structures like 6 or 7, with NO_2 (and NO_2^-) groups adsorbed on Cu^{2+} sites. At 150ºC nitrites desorb from the Cu^{2+} centers generating NO_2, as deduced from the decrease in the IR band at 1507 cm^{-1} and the concomitant increase in the band at 1668 cm^{-1} due to physisorbed NO_2 in Figure 13B. Subsequent increase of the temperature to 250º – 300ºC causes a decrease in the intensity of all bands, with those corresponding to nitrates (1578 cm^{-1}) being still observed at 350ºC. A new weak band at 1481 cm^{-1} appears at 250 and 350ºC associated to nitrate species as in structure 13 in Figure 8. The observation of nitrates at 150ºC agrees with the DFT results indicating that formation of nitrates from NO_2 involves higher activation energy barriers than initial formation of nitrites and NO_2.

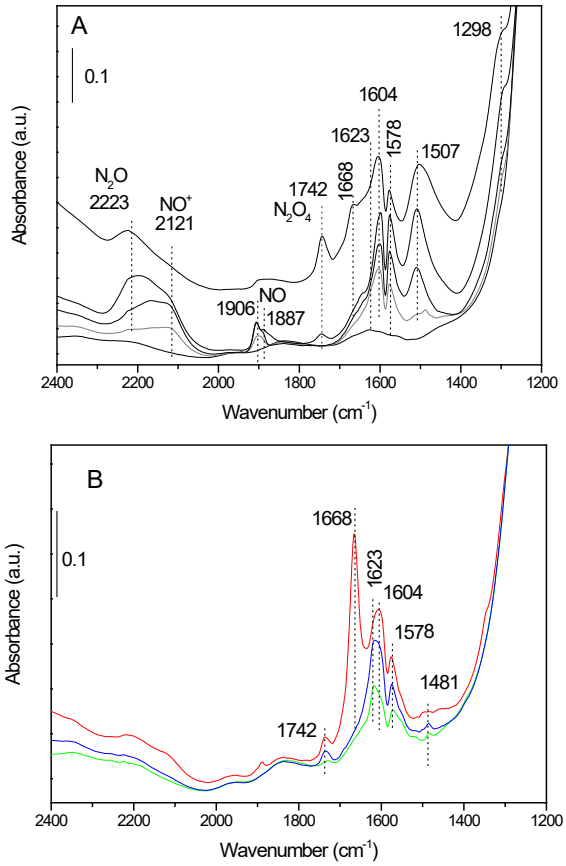

Figure 13. FTIR spectra of (A) NO adsorbed at 25ºC on Cu-SAPO-34 (gray line) and after O_2 co-adsorption ($2NO/5O_2/Cu$) with time (1, 16, 71min) (black lines) and (B) after increasing temperature in a $2NO/5O_2/Cu$ atmosphere at 150ºC (red line) 250ºC (blue line) and 350ºC (green line). Prior to adsorption the sample was preactivated in O_2 at 350ºC for 2h followed by vacuum at 150ºC for 1h.

The high stability of most nitrate and nitrite species formed by reaction of $NO+O_2$ toward evacuation is also shown in Figure 14. Only the species responsible for the signal at 1508 cm^{-1}, monodentate nitrite according to DFT simulations, desorbs completely at 150ºC, while the rest of bands are still clearly observed at 250 – 300ºC, in agreement with the EPR spectra in Figure 4.

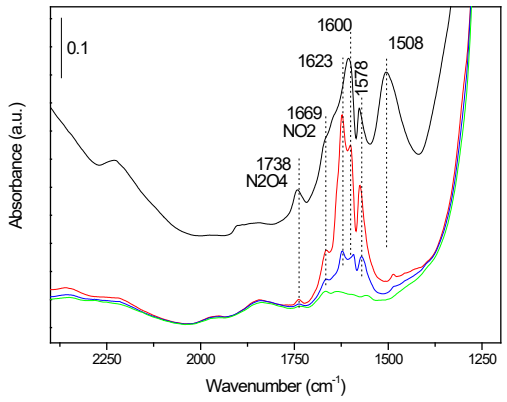

Figure 14. FTIR spectra of $2NO/5O_2/Cu$ adsorbed at 25ºC on Cu-SAPO-34 followed by vacuum treatment at different temperatures: 25ºC (black line), 150ºC (red line) 250ºC (blue line) and 350ºC (green line). The sample has been kept 30 min at each temperature. Prior to adsorption the sample was preactivated in O_2 at 350ºC for 2h followed by vacuum at 150ºC for 1h.

The IR spectra of Cu-SSZ-13 zeolite exposed to the same $NO+O_2$ mixture is quite different (Figure S18 in the Supporting Information). At 25ºC the most intense peaks appear at 1496 cm^{-1} and 1666 cm^{-1}, whereas the signals at 1610 and 1575 cm^{-1} observed in Cu-SAPO-34 and assigned to adsorbed NO_2 and NO_3^- species are relatively weak. According to DFT calculations (Table S6), NO_2^- species in the Cu-SSZ-13 sample would appear at higher frequency (~1525 cm^{-1}) discarding the assignation of the 1496 cm^{-1} IR band to nitrite, while it may correspond to some kind of monodentate nitrate species as depicted in structure 13, in agreement with Negri et al.[46] In addition to the above mentioned IR signals, bands at 1629, 1418 and 1379 cm^{-1} are also observed in Cu-SSZ-13, which are related to NO_2 molecules stabilized in the SSZ-13 zeolite channel (see Figure S19 in the Supporting Information). Further increase of the temperature to 150ºC does not modify the IR spectra in Figure S18, with the intensity of all bands remaining stable. Interestingly, the IR study suggests that, at low temperature, formation of Cu-nitrite is favored in Cu-SAPO-34 as compared to Cu-SSZ-13. Moreover, while Cu-nitrate interaction is strong in both Cu-SSZ-13 and Cu-SAPO-34 samples, the stability of Cu-nitrite is weak, producing NO_2 at 150ºC. The relatively higher amount of copper nitrites in Cu-SAPO-34 might be related its slightly higher catalytic activity in the low temperature range (Figure S1).

3. CONCLUSIONS

The *in situ* EPR spectra of Cu-SAPO-34 and Cu-SSZ-13 zeolites recorded in the presence of the reaction mixture ($NO+O_2+NH_3$) or ($NO+O_2$) at 230 ºC, a temperature just below maximum NO conversion in the NH_3-SCR-NO_x reaction, show a signal denoted here as $Cu^{2+}NO_x^-$ since, according to previous publications,[31] nitrate/nitrites are not discernable by EPR spectroscopy. $Cu^{2+}NO_x^-$ species are formed already at room temperature with $NO+O_2$ alone and also in the presence of ammonia, indicating that oxidation of Cu^+ cations to $Cu^{2+}NO_x^-$ occurs easily. This finding is confirmed by in situ IR spectroscopy, since bands associated to adsorbed NO_2, nitrites and nitrates are clearly observed at 25 ºC when Cu-SAPO-34 is exposed either to NO_2 alone or to a mixture of $NO+O_2$. Moreover, both EPR and IR spectroscopies show the formation of $Cu^{2+}NO_x^-$ species when the catalysts are exposed to NO alone, probably through a disproportionation pathway producing also N_2O, which is detected by IR.

The decresase in the relative intensity of the $Cu^{2+}NO_x^-$ EPR signal at 230 ºC - 250 ºC in the presence of the $NO+O_2+NH_3$ mixture when compared with $NO+O_2$ suggests that $Cu^{2+}NO_x^-$ participate in the NH_3-SCR- NO_x reaction in the low temperature region (T < 350 ºC). Regarding the particular role of NH_3 present under realistic SCR reaction conditions, our results indicate that it does not participate directly in the oxidation half-cycle. In the subsequent steps, NH_3 and/or NH_4^+ might assist in the desorption of the nitrite and/or nitrate species from Cu^{2+} forming NO_2NH_4 and/or NO_3NH_4, and is necessary to efficiently reduce Cu^{2+} to Cu^+ by reaction with $NO+NH_3$.

In this sense, $Cu^{2+}(NH_3)_x$ adducts, previously reported by our group when only ammonia is adsorbed on Cu-CHA zeolites, [31] are not detected in the presence of the reaction mixture ($NO+O_2+NH_3$), further supporting that Cu^+ cations directly attached to framework oxygen atoms of the CHA structure can be oxidized to Cu^{2+} by $NO+O_2$ at low temperature, without the direct participation of ammonia.

From the DFT study several pathways are proposed to oxidize Cu^+ cations located in the 6R rings of the CHA structure and connected to framework oxygen atoms by reaction with $NO+O_2$. These pathways generate adsorbed NO_2 and NO_2^- species with activation energy barriers between 55 and 70 kJ mol^{-1}, and are kinetically relevant already at room temperature. Formation of $Cu^{2+}NO_3^-$ species requires activation energies larger than 96 kJ mol^{-1}, which agrees with the observation of IR bands associated to $Cu^{2+}NO_3^-$ species preferentially at 150 ºC.

The experimental evidence on the low temperature oxidation of Cu^+ with NO + O_2 to form Cu^{2+}-nitrites/nitrates without requiring the participation of ammonia presented here appears to be in contradiction with the more recent reaction model invoking the formation of transient dimeric $[Cu^{2+}(NH_3)_2]$-O_2-$[Cu^{2+}(NH_3)_2]$ intermediates from mobile $Cu^+(NH_3)_2$ species.[22-25] This model is founded on the statement that Cu^+ and Cu^{2+} are coordinated to NH_3 molecules under reaction conditions (based on the simulation of the XAFS spectra)[22, 25] and on the too high activation energies for the direct oxidation of Cu^+ attached to the zeolite to $Cu^{2+}NO_3^-$ reported in the bibliography.[17, 19, 39] New DFT calculations showed that the direct oxidation of $Cu^+(NH_3)_2$ complexes requires too high E_a (175 kJ mol^{-1}) to fit experimental results, but that the barrier is considerably reduced, falling within the range of the experimental values, when dimers are considered (76 kJ mol^{-1}) [24] In this work, similar activation energy values between 55 and 70 kJ mol^{-1} are obtained for the oxidation of ammonia-free Cu^+ cations directly attached to framework oxygens, and these barriers are practically not affected when also NH_3 is included in the calculations.

Although the mechanism proposed here would not explain the square dependence on Cu loading observed only at low T (200ºC) for samples with relatively high Al content and very low Cu loading (Cu/Al < 0.03),[24] it matches the experimental data reported for Cu-SSZ-13 catalysts with a Cu/Al ratio higher than ~0.05, that is, for most samples used in most experimental studies including the present one ((Cu/Al ~0.6 for Cu-SSZ-13 and Cu/Si ~0.5 for Cu-SAPO-34). These experimental data give activation energies around 70-80 kJ/mol and a linear dependence of the reaction rate on Cu loading, both explained with the proposed mechanism.

In summary, the results presented here demonstrate that a reaction mechanism invoking the formation of nitrate/nitrite intermediates on copper cations attached to the zeolite framework without requiring the participation of ammonia in the oxidation half-cycle can be operational in the low temperature region (T < 350 ºC). Moreover, different intermediate species are predominantly observed in the two catalysts studied, nitrites in Cu-SAPO-34 and nitrates in Cu-SSZ-13. While the role of nitrate species in the catalytic pathway is still uncertain, this difference could be related to the slightly lower reactivity observed in the Cu-SSZ-13 sample at low temperature.

4. EXPERIMENTAL SECTION

4.1. Synthesis of Cu-zeolites. Zeolite Cu-SSZ-13 was prepared by one-pot direct synthesis using a method developed by our group and described previously,[27] from a synthesis gel of chemical composition: SiO_2 : 0.062 Al_2O_3 : 0.1 Na_2O : 0.06 Cu-TEPA : 0.15 TMAdaOH : 21 H_2O, being Cu-TEPA: copper-tetraethylethylene-pentamine, TMAdaOH: N,N,N-trimethyl-1-adamantammonium hydroxide. The gel was introduced into an autoclave with a Teflon liner and heated at 150ºC under static conditions for 14 days. The resulting crystalline products were filtered and washed with water, dried at 100ºC, and then calcined at 550ºC in air to remove the occluded organic material.

Cu-SAPO-34 material was also prepared by one-pot direct synthesis using a method developed by our group and described previously,[28] from a synthesis gel of chemical composition: 0.19 SiO_2 : 0.5 Al_2O_3 : 0.4 P_2O_5 : 0.045 Cu-TEPA : 0.855 DEA : 18 H_2O, being DEA: diethylamine. The gel was introduced into an autoclave with a Teflon liner containing SAPO-34 seeds as well, and heated at 150ºC under static conditions for 5 days. The resulting crystalline products were filtered and washed with water, dried at 100ºC, and then calcined at 550ºC in air to remove the occluded organic material. The chemical composition of the obtained materials was analyzed by ICP-O ES (Varian 715-ES), and the results are reported in Table S1.

4.2. Catalytic tests. Catalytic tests were carried out in a fixed bed quartz tubular reactor of 1.2 cm of diameter and 20 cm length, where 40 mg of catalyst were introduced. Firstly, the catalyst was pre-treated at 500 °C under N_2 flow (300 ml/min) for 1h. Next, the desired temperature was set (170 – 550°C) and the flow changed to the reaction feed consisting of: 300 ml/min of a mixture composed by 500 ppm of NO, 530 ppm of NH_3, 7% of O_2, 5% of H_2O and N_2 as balance gas. The reaction was followed by the conversion of NO that was analyzed with a chemiluminescence detector Eco Physiscs 62c. The results in Figure S1 show that both samples are highly active from 200ºC to 550ºC, but especially in the 250 ºC – 450 °C range where the NO conversion is over 99%.

4.3. EPR experiments. About 20 mg of Cu-zeolite was placed into a 5 mm EPR quartz tube adapted to a high vacuum valve, connected to a vacuum line and dehydrated under dynamic vacuum at 450 °C (1 h) reaching a final pressure of ~10^{-6} mbar. Next, 99.9% isotopically labelled ^{15}NO, $^{15}NO/O_2$ or $^{15}NO/NH_3/O_2$ were adsorbed at -196°C by admitting onto the Cu-zeolite the desired amount of gas using a calibrated volume. Then the EPR spectra were measured at the desired temperatures (see below). Finally, in some cases, as stated in the text, the sample with the adsorbed gases in the quartz tube was further degassed in the vacuum line at temperatures between 25 – 450° C and the spectra was measured afterwards. Labelled ^{15}NO instead of NO was used because of the higher gas purity.

EPR spectra were recorded with a Bruker EMX-12 spectrometer, operating at the X-band, with a modulation frequency of 100 KHz and amplitude of 1.0 Gauss. Spectra were measured at variable temperatures (-170 – 230 °C) using a Variable Temperature Accessory working with liquid or gas N_2 depending on the temperature of measurement.

4.4. Computational Details. Periodic density functional calculations were performed using the Perdew-Wang (PW91) exchange-correlation functional within the generalized gradient approach (GGA)[48,49] as implemented in the VASP code.[50,51] The valence density was expanded in a plane wave basis set with a kinetic energy cutoff of 450 eV, and the effect of the core electrons in the valence density was taken into account by means of the projected augmented wave (PAW) formalism.[52] Integration in the reciprocal space was carried out at the Γ k-point of the Brillouin zone. Electronic energies were converged to 10^{-6} eV and geometries were optimized until forces on atoms were less than 0.01 eV/Å. Transition states were obtained using either the DIMER algorithm.[53,54] During geometry optimizations the positions of all atoms in the system were allowed to relax without any restriction. Vibrational frequencies were calculated by diagonalizing the block Hessian matrix corresponding to displacements of the Cu, N, H and O atoms not belonging to the catalyst framework.

The chabazite structure was modelled by means of a hexagonal unit cell with lattice parameters a = b = 13.8026 Å, c = 15.0753 Å, α = β = 90º and γ = 120º containing 72 O atoms and either 36 Si or 18 Al and 18 P atoms. To generate the Cu-SSZ-13 and Cu-SAPO-34 models, two framework Si or P atoms were substituted by Al or Si atoms, respectively, (Si/Al and (Al+P)/Si ratio = 17) and a Cu^+ cation was placed in a 6R ring with a Brönsted acid site nearby to keep the system neutral. The 6R, 6RB and D6R distributions of Al in Cu-SSZ-13 and the 6R and D6R Si positions in Cu-SAPO-34 shown in Figure 1 were used in the mechanistic study.

The relative stability (E_{rel}) of all structures involved in the oxidation of Cu^+ to Cu^{2+} by NO + O_2 was calculated according to:

$$E_{rel} = E_{structure} - E_{Cu\text{-}CHA} - 2E_{NO} - E_{O2}$$

where Estructure, $E_{Cu\text{-}CHA}$, E_{NO} and E_{O2} are the total energies of the structure considered, the Cu-CHA catalyst, NO and O_2, respectively. Activation and reaction energies for each elementary step were calculated as the energy difference between the transition state (TS) or the product (P) of the process and the corresponding reactant (R) structure for that step.

$$E_{act} = E_{TS} - E_R$$
$$E_{reac} = E_P - E_R$$

Finally, adsorption K_{ads} and kinetic rate k_r constants for the most relevant steps were derived from calculated adsorption ΔG_{ads} and activation ΔG_{act} Gibbs free energies, respectively, as follows:

$$K_{ads} = e^{-\Delta G_{ads}/RT}$$
$$k_r = \left(\frac{k_B T}{h}\right) e^{-\Delta G_{act}/RT}$$

The calculation of absolute Gibbs free energies is described in detail in the Supporting Information.

4.5. IR spectroscopy. IR spectra were recorded with a Bruker spectrometer, Vertex 70, using a DTGS detector and acquiring at 4 cm^{-1} resolution. An IR cell allowing in situ treatments in controlled atmospheres and temperatures from 25ºC to 500ºC was connected to a vacuum system with gas dosing facility. For IR studies the samples were pressed into self-supported wafers and treated in O_2 flow for 2h at 350ºC followed by vacuum (10^{-4} mbar) treatment at 150ºC for 1 h or under dynamic vacuum (10^{-4} mbar) at 450ºC for 1h. After activation, the sample was cooled down in vacuum to 25ºC. In the NO+O_2 experiments, NO ($1.4*10^{-5}$ mol) and O_2 ($3.1*10^{-5}$ mol), corresponding to a molar ratio 2NO/5O_2/Cu, were dosed at 25ºC. Spectra were acquired at 25ºC and at increasing temperatures of 150ºC, 250ºC and 350ºC. In another set of experiments and in order to study the stability of the intermediate species formed in the NO+O_2 reaction, after NO+O_2 dosing at 25ºC, the sample was submitted to vacuum (10^{-4} mbar) and increasing temperatures under dynamic vacuum conditions.

In the NO_2 adsorption experiments, NO_2 was adsorbed on the pre-activated samples at 25ºC and at increasing dosing ($1.5*10^{-5}$ mol to 11.2*10-5 mol) until saturation.

4.6. Raman spectroscopy. Raman spectra were recorded with a 785 nm laser excitation on a Renishaw Raman Spectrometer ("in

via") equipped with a CCD detector. The laser power on the sample was 25 mW and a total of 20 acquisitions were taken for each spectra. The sample has been pre-activated in O_2 flow at 230ºC and then flushed with N_2 at the same temperature. Spectra have been acquired under both O_2 and N_2 conditions.

ASSOCIATED CONTENT

Supporting Information

Details of calculation of Gibbs free energies. Chemical composition and catalytic activity of Cu-SSZ-13 and Cu-SAPO-34 samples. EPR parameters at different T and EPR spectra of NO adsorption on Cu-SAPO-34. Relative stability of different Cu and Si distributions in Cu-SAPO-34. DFT calculated kinetic constants for gas phase reactions and vibrational frequencies for relevant intermediates. DFT geometries and energy profiles for different sites in Cu-SAPO-34 and Cu-SSZ-13 models. Raman and FTIR spectra for Cu-SAPO-34 with different preactivation and for H-SAPO-34, Cu-SSZ-13 and H-SSZ-13 samples.

AUTHOR INFORMATION

Corresponding Autthor
Mercedes Boronat, boronat@itq.upv.es
Teresa Blasco, tblasco@itq.upv.es

ORCID
Mercedes Boronat: 0000-0002-6211-5888
Patricia Concepción: 0000-0003-2058-3103
Teresa Blasco: 0000-0002-8115-4241

Notes
The authors declare no competing financial interest.

ACKNOWLEDGMENT

This work was supported by the Spanish Government through "Severo Ochoa Program" (SEV 2012-0267; SEV-2016-0683), MAT2015-71261-R and CTQ2015-68951-C3-1-R, and by the European Union through ERC-AdG-2014-671093 (SynCatMatch). Red Española de Supercomputación (RES) and Centre de Càlcul de la Universitat de Valencia are gratefully acknowledged for computational resources and technical support. R. M. acknowledges "La Caixa – Severo Ochoa" International PhD Fellowships (call 2015).

REFERENCES

(1) Chen, H.-Y. In *Urea-SCR Technology for deNOx After Treatment of Diesel Exhausts*; Nova, I., Tronconi, E., Eds.; Springer: New York, **2014**; pp 123–147.
(2) Brandenberger, S.; Krocher, O.; Tissler, A.; Althoff, R.; Kröcher, O. *Catal. Rev. Sci. Eng*. **2008**, 50, 492.
(3) Gao, F.; Kwak, J.; Szanyi J.; Peden, C. H. F. Current Understanding of Cu-Exchanged Chabazite Molecular Sieves for Use as Commercial Diesel Engine DeNOx Catalysts. *Topics in Catal.* **2013**, 56, 1441–1459.
(4) Beale, A. M.; Gao, F.; Lezcano-Gonzalez, I.; Peden, C. H. F.; Szanyi, J. Recent Advances in Automotive Catalysis for NOx Emission Control by Small-Pore Microporous Materials. *Chem. Soc. Rev.* **2015**, 44, 7371–7405.
(5) Zhang, R.; Liu, N.; Lei, Z.; Chen, B. Selective Transformation of Various Nitrogen-Containing Exhaust Gases toward N_2 over Zeolite Catalysts. *Chem. Rev.* **2016**, 116(6), 3658–3721.
(6) Kwak, J. H.; Tonkyn, R. G.; Kim, D. H.; Szanyi, J.; Peden, C. H. F. Excellent Activity and Selectivity of Cu-SSZ-13 in the Selective Catalytic Reduction of NOx with NH_3. *J. Catal.* **2010**, 275, 187–190.
(7) Fickel, D. W.; D'Addio, E.; Lauterbach, J. A.; Lobo, R. F. The Ammonia Selective Catalytic Reduction Activity of Copper-Exchanged Small-Pore Zeolites. *Appl. Catal. Environ.* **2011**, 102, 441–448.
(8) Deka, U.; Lezcano-González, I.; Weckhuysen, B. M.; Beale, A. M. Local Environment and Nature of Cu Active Sites in Zeolite-Based Catalysts for the Selective Catalytic Reduction of NOx. *ACS Catal.* **2013**, 3, 413–427.
(9) Paolucci, C.; Di Iorio, J. R.; Ribeiro, F. H.; Gounder, R.; Schneider, W. F. Catalysis Science of NOx Selective Catalytic Reduction with Ammonia Over Cu-SSZ-13 and Cu-SAPO-34. *Advances in Catalysis* **2016**, 59, 1-107.
(10) Fickel, D. W.; Lobo, R. Copper Coordination in Cu-SSZ-13 and Cu-SSZ-16 Investigated by Variable-Temperature XRD. *J. Phys. Chem. C* **2010**, 114, 1633–1640.
(11) Borfecchia, E.; Beato, P.; Svelle, S.; Olsbye, U.; Lamberti, C.; Bordiga, S. Cu-CHA - A Model System for Applied Selective Redox Catalysis. *Chem. Soc. Rev.* **2018**, *47*, 8097– 8133.
(12) Paolucci, C.; Parekh, A. A.; Khurana, I.; Di Iorio, J. R.; Li, H.; Albarracin Caballero, J. D.; Shih, A. J.; Anggara, T.; Delgass, W. N.; Miller, J. T.; Ribeiro, F. H.; Gounder, R.; Schneider, W. F. Catalysis in a Cage: Condition-Dependent Speciation and Dynamics of Exchanged Cu Cations in SSZ-13 Zeolites. *J. Am. Chem. Soc.* **2016**, 138, 6028–6048.
(13) Bates, S. A.; Verma, A. A.; Paolucci, C.; Parekh, A.; Anggara, T.; Schneider, W. F.; Miller, J. T.; Delgass, W. N.; Ribeiro, F. H. Identification of the Active Cu Site in Standard Selective Catalytic Reduction with Ammonia on Cu-SSZ-13. *J. Catal.* **2014**, 312, 87–97.
(14) Beale, A. M.; Lezcano-Gonzalez, I.; Slawinksi, W. A.; Wragg, D. S. Correlation between Cu Ion Migration Behaviour and deNO(x) Activity in Cu-SSZ-13 for the Standard NH_3-SCR Reaction. *Chem. Commun*., **2016**, 52, 6170–6173
(15) Paolucci, C.; Verma, A. A.; Bates, S. A.; Kispersky, V. F.; Miller, J. T.; Gounder, R.; Delgass, W. N.; Ribeiro, F. H.; Schneider, W. F. Isolation of the Copper Redox Steps in the Standard Selective Catalytic Reduction on Cu-SSZ-13. *Angew. Chem. Int. Ed.* **2014**, 53, 11828–11833
(16) Lomachenko, K. A; Borfecchia, E.; Negri, C.; Berlier, G.; Lamberti, C.; Beato, P.; Falsig, H.; S. Bordiga. The Cu-CHA deNO(x) Catalyst in Action: Temperature-Dependent NH_3-Assisted Selective Catalytic Reduction Monitored by Operando XAS and XES. *J. Am. Chem. Soc.* **2016**, 138, 12025−12028.
(17) Janssens, T. V. W.; Falsig, H.; Lundegaard, L. F.; Vennestrøm, P. N. R.; Rasmussen, S. B.; Moses, P. G.; Giordanino, F.; Borfecchia, E.; Lomachenko, K. A.; Lamberti, C.; Bordiga, S.; Godiksen, A.; Mossin, S.; Beato, P. A Consistent Reaction Scheme for the Selective Catalytic Reduction of Nitrogen Oxides with Ammonia. *ACS Catal.* **2015**, 5, 2832–2845.
(18) Di Iorio, J. R.; Bates, S. A.; Verma, A. A.; Delgass, W. N.; Ribeiro, F. H.; Miller, J. T.; Gounder, R. The Dynamic Nature of Brønsted Acid Sites in Cu–Zeolites During NOx Selective Catalytic Reduction: Quantification by Gas-Phase Ammonia Titration. *Top. Catal.* **2015**, 58, 424–434.
(19) Mao Y.; Wang, Z.; Wang, H-F, Hu, P. Understanding Catalytic Reactions over Zeolites: A Density Functional Theory Study of Selective Catalytic Reduction of NOx by NH_3 over Cu-SAPO-34. *ACS Catal.* **2016**, *6, 7882.*
(20) Wang, D.; Zhang, L.; Kamasamudram, K.; Epling, W. S. In Situ-DRIFTS Study of Selective Catalytic Reduction of NOx by NH_3 over Cu-Exchanged SAPO-34. *ACS Catal.* **2013**, 3, 871-881.
(21) Gao, F.; Washton, N. M.; Wang, Y.; Kollar, M.; Szanyi, J.; Peden, C. H. F. Effects of Si/Al Ratio on Cu/SSZ-13 NH_3-SCR Catalysts: Implications for the Active Cu Species and the Roles of Brønsted Acidity. *J. Catal.* **2015**, 331, 25–38.
(22) Paolucci, C.; Khurana, I.; Parekh, A. A.; Li, S.; Shih, A. J.; Li, H.; Di Iorio, J. R.; Albarracin-Caballero, J. D.; Yezerets, A.;

Miller, J. T.; Delgass, W. N.; Ribeiro, F. H.; Schneider, W. F.; Gounder, R. Dynamic Multinuclear Sites Formed by Mobilized Copper Ions in NOx Selective Catalytic Reduction. *Science* **2017**, 357, 898–903.
(23) Chen, L.; Falsig, H.; Janssens T. V. W.; Grönbeck, H. Activation of Oxygen on (NH_3-Cu-NH_3)(+) in NH_3-SCR over Cu-CHA. *J. Catal.* **2018**, 358, 179-186
(24) Gao, F.; Mei, D.; Wang, Y.; Szanyi, J.; Peden, C. H. F. Selective Catalytic Reduction over Cu/SSZ-13: Linking Homo- and Heterogeneous Catalysis. *J. Am. Chem. Soc.* **2017**, 139, 4935–4942.
(25) Marberger, A.; Petrov, A. W.; Steiger P.; Elsener, M.; Kröcher, O.; Nachtegaal, M; Ferri, D. Time-Resolved Copper Speciation during Selective Catalytic Reduction of NO on Cu-SSZ-13 *Nature Catal.* **2018**, 1, 221-227.
(26) Moreno-González, M.; Palomares, A. E.; Chiesa, M.; Boronat, M.; Giamello, E.; Blasco, T. Evidence of a Cu^{2+}–Alkane Interaction in Cu-Zeolite Catalysts Crucial for the Selective Catalytic Reduction of NOx with Hydrocarbons. *ACS Catal.* **2017**, 7, 3501–3509.
(27) Martinez-Franco, R.; Moliner, M.; Thogersen, J. R.; Corma, A. Efficient One-Pot Preparation of Cu-SSZ-13 Materials Using Cooperative OSDAs for their Catalytic Application in the SCR of NOx. *ChemCatChem* **2013**, 5, 3316–3323.
(28) Martinez-Franco, R.; Moliner, M.; Concepción, P.; Thogersen, J. R.; Corma, A. Synthesis, Characterization and Reactivity of High Hydrothermally Stable Cu-SAPO-34 Materials prepared by "one-pot" Processes. *J. Catal.* **2014**, 314, 73–82.
(29) Godiksen, A.; Vennestrom P. N. R.; Rasmussen, S.; Mossin, S. Identification and Quantification of Copper Sites in Zeolites by Electron Paramagnetic Resonance Spectroscopy. *Topics in Catal.* **2017**, 60, 13–29.
(30) Godiksen, A.; Isaksen, O. L.; Rasmussen, S. B.; Vennestrom P. N. R.; Mossin, S. Site-Specific Reactivity of Copper Chabazite Zeolites with Nitric Oxide, Ammonia, and Oxygen. *ChemCatChem* **2017**, 10, 366–370.
(31) Fernández, E.; Moreno-González, M.; Moliner, M.; Blasco, T.; Boronat, M.; Corma, A. Modeling of EPR Parameters for Cu(II): Application to the Selective Reduction of NOx Catalyzed by Cu-Zeolites. *Topics in Catal.* **2018**, *61*, 810–832.
(32) Moreno-González, M.; Hueso, B.; Boronat, M.; Blasco, T.; Corma, A. Ammonia-Containing Species Formed in Cu-Chabazite As Per In Situ EPR, Solid-State NMR, and DFT Calculations. *J. Phys. Chem. Lett.* **2015**, *6*, 1011–1017.
(33) Giamello, E.; Murphy, D.; Magnacca, G.; Morterra, C.; Shioya, Y.; Nomura, T.; Anpo, M. The Interaction of NO with Copper Ions in ZSM5: An EPR and IR Investigation. *J. Catal.* **1992**, 136, 510 –520.
(34) Spoto, G.; Bordiga, S.; Scarano, D.; Zecchina, A.; *Catal. Lett.* 1992, *13*, 39–44.
(35) G. Spoto, G.; Zecchina, A.; Bordiga, S.; Ricchiardi, G.; Martra, G.; Leofanti, G.; Petrini, G. *Appl. Catal. B* **1994**, *3*, 151–172.
(36) Lamberti, C.; Bordiga, S.; Salvalaggio, M.; Spoto, G.; Zecchina, A.; Geobaldo, F.; Vlaic, G.; Bellatreccia, M. *J. Phys. Chem. B* **1997,** *101,* 344– 360.
(37) Pulido, A.; Nachtigall, P. Correlation Between Catalytic Activity and Metal Cation Coordination: NO Decomposition Over Cu/Zeolites. *ChemCatChem* **2009**, *1*, 449 – 453.
(38) Pulido, A.; Nachtigall, P. Theoretical investigation of dinitrosyl complexes in Cu-zeolites as intermediates in deNOx process. *Phys. Chem. Chem. Phys*. **2009**, *11*, 1447–1458.
(39) Falsig, H.; Vennestrom, P. N. R.; Moses, P. G.; Janssens, T. V. W. Activation of Oxygen and NO in NH_3-SCR over Cu-CHA Catalysts Evaluated by Density Functional Theory. *Top. Catal.* **2016**, 59, 861–865.
(40) Concepción, P.; Boronat, M.; Millán, R.; Moliner, M.; Corma, A. Identification of Distinct Copper Species in Cu-CHA Samples Using NO as Probe Molecule. A Combined IR Spectroscopic and DFT Study. *Top.Catal.* **2017**, 60, 1653–1663.
(41) Artioli, N.; Lobo, R.; Iglesia, E. Catalysis by Confinement: Enthalpic Stabilization of NO Oxidation Transition States by Microporororous and Mesoporous Siliceous Materials. *J. Phys. Chem. C* **2013**, *117*, 20666 –20674.
(42) Maestri, M.; Iglesia, E. , First-principles Theoretical Asessment of Catalysis by Confinement: NO–O2 Reactions within Voids of Molecular Dimensions in Siliceous Crystalline Frameworks. *Phys. Chem. Chem. Phys.* **2018**, *20*, 15725–15735.
(43) Bin, F.; Song, C.; Lv, G.; Song, J.; Wu, S.; Li, X. Selective Catalytic Reduction of Nitric Oxide with Ammonia over Zirconium-Doped Copper/ZSM-5 Catalysts. *Appl. Catal. B. Env.* **2014**, 150-151, 532-543.
(44) Liu, Z.; Zhang, S.; Li, J.; Ma; L. Promoting Effect of MoO_3 on the NOx Reduction by NH_3 over CeO_2/TiO_2 Catalyst Studied with in situ DRIFTS. *Appl. Catal B. Env.* **2014**, 144, 90-95.
(45) Tamm, S.; Vallim, N.; Skoglundh, M.; Olsson, L. The Influence of Hydrogen on the Stability of Nitrates during H_2-Assisted SCR over Ag/Al_2O_3 Catalysts – A DRIFT Study. *J. Catal.* **2013**, 307, 153-161.
(46) Negri, C.; Hammershöi, P. S.; Janssens, T. V. W.; Beato, P.; Berlier, G.; Bordiga, S. Investigating the Low Temperature Formation of CuII-(N,O) Species on Cu-CHA Zeolites for the Selective Catalytic Reduction of NOx. Chem. Eur. J. 2018, 12044–12053.
(47) Woertink, J. S.; Smeets, P. J.; Groothaert, M. H.; Vance, M. A.; Sels, B. F.; Schoonheydt, R. A.; Solomon, E. I. A $(Cu_2O)^{2+}$ core in Cu-ZSM-5, the active site in the oxidation of methane to metanol. *PNAS* **2009**, 106, 18908-18913.
(48) Perdew, J. P.; Chevary, J. A.; Vosko, S. H.; Jackson, K. A.; Pederson, M. R.; Singh, D. J.; Fiolhais, C. Atoms, Molecules, Solids, and Surfaces: Applications of the Generalized Gradient Approximation for Exchange and Correlation. *Phys. Rev. B* **1992**, 46, 6671–6687.
(49) Perdew, J. P.; Wang, Y. Accurate and Simple Analytic Representation of the Electron-Gas Correlation Energy. *Phys. Rev. B* **1992**, 45, 13244–13249.
(50) Kresse, G.; Furthmüller. Efficient Iterative Schemes for Ab Initio Total-Energy Calculations Using a Plane-Wave Basis Set. J. *Phys. Rev. B* **1996**, 54, 11169–11186.
(51) Kresse, G.; Hafner. Ab Initio Molecular Dynamics for Liquid Metals. J. *Phys. Rev. B* **1993**, 47, 558–561.
(52) Blöchl, P. E. Projector Augmented-Wave Method. *Phys. Rev. B* **1994**, 50, 17953–17979.
(53) Henkelman, G.; Jonsson, H. A Dimer Method for Finding Saddle Points on High Dimensional Potential Surfaces using Only First Derivatives. *J. Chem. Phys.* **1999**, 111, 7010–7022.
(54) Heyden, A.; Bell, T.; Keil, F. J. Efficient Methods for Finding Transition States in Chemical Reactions: Comparison of Improved Dimer Method and Partitioned Rational Function Optimization Method. *J. Chem. Phys*. **2005**, 123, 224101–224114.

Spectroscopic Evidence and DFT Analysis of Low Temperature Oxidation of Cu^{+} to $Cu^{2+}NO_x$ in Cu-CHA Catalysts. Implications for the SCR-NO_x Reaction Mechanism

Marta Moreno-González,[†,‡] Reisel Millán,[†] Patricia Concepción, Teresa Blasco[*] and Mercedes Boronat[*]

Instituto de Tecnología Química, Universitat Politècnica de València - Consejo Superior de Investigaciones Cientificas, Av. de los Naranjos, s/n, 46022 Valencia, Spain

[‡]Present address: Deparment of Chemistry, The University of British Columbia, 2036 Main Mall, Vancouver, British Columbia V6H1Z1, Canada

[†]These authors contributed equally to this work

Insert Table of Contents artwork here